second paper[1] between the model and experimental data in the $Pb_{1-x}Sn_xTe$ system. Among these quantities of interest is the Knight shift. The theory of the Knight shift is developed in the context of the Landau levels appropriate to these materials, including the identification of an inhomogeneous broadening of the NMR line produced by the orientation dependence of the Landau-level wave function.

ACKNOWLEDGMENTS

The authors wish to thank Professor Arthur C. Smith, Professor Mildred Dresselhaus, and Professor Peter Wolff for many helpful discussions.

†Work supported by Office of Naval Research and Advanced Research Projects Agency.

*This paper is based in part on the Doctoral thesis of M. S. Adler (MIT, 1971).

‡Present address: General Electric Co. Schenectady, N. Y.

[1]C. R. Hewes, M. S. Adler, and S. D. Senturia, following paper, Phys. Rev. B **7**, 5195 (1973).

[2]M. H. Cohen, Phys. Rev. **121**, 387 (1961).

[3]S. D. Senturia, A. C. Smith, C. R. Hewes, J. A. Hofmann, and P. L. Sagalyn, Phys. Rev. B **1**, 4045 (1970).

[4]C. R. Hewes, Ph.D. thesis (MIT, Department of Electrical Engineering, 1970) (unpublished).

[5]M. S. Adler, Ph.D. thesis (MIT, Department of Electrical Engineering, 1971) (unpublished).

[6]S. D. Senturia, A. C. Smith, C. R. Hewes, M. S. Adler, J. A. Hofmann, and P. L. Sagalyn, J. Phys. Chem. Solids Suppl. **32**, 333 (1971).

[7]J. B. Conklin, Jr., L. E. Johnson, and G. W. Pratt, Jr., Phys. Rev. **137**, A1282 (1965).

[8]S. Rabii, Phys. Rev. **167**, 801 (1968).

[9]P. J. Lin and L. Kleinman, Phys. Rev. **142**, 478 (1966).

[10]R. L. Bernick, Ph.D thesis (University of Southern California, Department of Physics, 1970).

[11]R. L. Bernick and L. Kleinman, Solid State Commun. **8**, 569 (1970).

[12]S. Rabii, Phys. Rev. **182**, 821 (1969).

[13]Y. W. Tung and M. L. Cohen, Phys. Rev. **180**, 823 (1969).

[14]Y. W. Tung and M. L. Cohen, Phys. Lett. **29A**, 236 (1967).

[15]J. O. Dimmock, I. Melngailis, and A. J. Strauss, Phys. Rev. Lett. **16**, 1193 (1966).

[16]J. O. Dimmock, J. Phys. Chem. Solids Suppl. **32**, 319 (1971).

[17]D. L. Mitchell and R. F. Wallis, Phys. Rev. **151**, 581 (1966).

[18]J. M. Luttinger and W. Kohn, Phys. Rev. **97**, 869 (1955).

[19]B. Lax and J. G. Mavroides, in *Solid State Physics*, edited by F. Seitz and D. Turnbull, (Academic, New York 1960), Vol. II, p. 261.

[20]P. A. Wolff, J. Phys. Chem. Solids **25**, 1057 (1969).

[21]G. A. Baraff, Phys. Rev. **137**, A842 (1965).

PHYSICAL REVIEW B VOLUME 7, NUMBER 12 15 JUNE 1973

Nuclear-Magnetic-Resonance Studies in PbTe and $Pb_{1-x}Sn_xTe$: An Experimental Determination of $\vec{k}\cdot\vec{p}$ Band Parameters and Magnetic Hyperfine Constants*†

C. Robert Hewes, Michael S. Adler‡, and Stephen D. Senturia

Center for Materials Science and Engineering, and Department of Electrical Engineering, Massachusetts Institute of Technology, Cambridge, Massachusetts 02139

(Received 27 July 1972)

Measurements are reported of the Knight shifts of Pb^{207} and Sn^{119} in 61 samples of PbTe and $Pb_{1-x}Sn_xTe$ as functions of carrier concentration, alloy composition, and temperature. The results are interpreted in terms of a quantitative six-band $\vec{k}\cdot\vec{p}$ band model for the magnetic energy levels of the valence and conduction bands. All available experimental data pertaining to effective masses and g factors are examined using this model, including the results of magneto-oscillatory, magneto-optical, and other Fermi-surface studies. Remarkable agreement with published data and with the NMR data is obtained with principal matrix elements of momentum which are independent of composition. The temperature dependence of the Knight shift up to 100 K is understood in terms of the changing carrier degeneracy, but above 100 K an additional temperature dependence is observed. Unexplained structure is reported in the temperature dependence of the Knight shifts in alloy samples near their band inversions. Contact interaction and orbital hyperfine constants are reported. The orbital hyperfine constants are surprisingly large in these materials. In addition, the magnitude of the hyperfine coupling depends on alloy composition.

I. INTRODUCTION

This paper reports the results of an extensive nuclear-magnetic-resonance (NMR) study of PbTe[1] and $Pb_{1-x}Sn_xTe$ alloys[2] for $x \lesssim 0.6$. An important outgrowth of this work has been the development in an earlier paper[3] of a unified $\vec{k}\cdot\vec{p}$ band model for these compound semiconductors. In the present paper, this model is used in full quantitative detail to interpret not only the NMR data, but also a broad

spectrum of data having bearing on the details of the energy-band extrema and the Fermi surface at low temperatures. The results of this analysis are a set of $\vec{k}\cdot\vec{p}$ coupling parameters from which effective masses, g factors, and all quantities depending on them can be calculated with an accuracy which agrees with experiment. In addition, hyperfine coupling constants between the carriers and the Pb^{207} and Sn^{119} nuclei are obtained. The magnitude of some of these constants are surprisingly large, and they show a variation with alloy composition which remains unexplained.

Interest in the lead-salt semiconductors (PbS, PbSe, PbTe, and their alloys with related Sn compounds) has stemmed from two sources: the broad applicability of these narrow-gap, direct-gap materials to infrared devices, and the discovery of a rich lode of interesting physics problems, many of which are related to the presence, even the dominance of relativistic effects in certain features of the energy-band structure. Both augmented-plane-wave (APW)[4,5] and pseudopotential[6-8] band calculations in PbTe and SnTe have affirmed the important contribution of spin-orbit couplings and other relativistic interactions to the band ordering. Furthermore, the variation in spin-orbit energy between the PbTe and SnTe has been cited as the basis for the proposed crossing of the valence and conduction bands at an intermediate alloy composition.[9] Without spin-orbit couplings only the longitudinal momentum matrix elements across the L-point gap would be nonzero. However, the strong spin-orbit mixing is responsible for nonzero transverse momentum matrix elements as well. These matrix elements and the small energy gap give rise to small effective masses and large g factors. These, when coupled with the large hyperfine constants to be expected in heavy nuclei, lead to the expectation of large Knight shifts, an expectation which has been indeed been borne out by experiment.

The first NMR measurements in lead telluride were reported by Weinberg[10,11] and by Weinberg and Callaway.[12] Their measurements of the Pb^{207} resonance in a single p-type sample covered the temperature range from 250 to 450 K. Sapoval used helicon-wave NMR methods[13] to determine the Pb^{207} Knight shift at liquid-helium temperatures in p-type PbTe.[14] His data and his relatively simple model are in general agreement with the results of our studies. Two reports of our own preliminary work have appeared, the first on PbTe,[15] the second on $Pb_{1-x}Sn_xTe$.[16] Related measurements of the Pb^{207} resonance in PbSe have been reported by Lee, Liesegang, and Phipps.[17] A much more extensive study of PbSe is currently under way in Sapoval's laboratory.[18]

We have studied Pb^{207} nuclear resonances in more than 60 samples of PbTe and $Pb_{1-x}Sn_xTe$ covering the composition range from pure PbTe to $Pb_{0.4}Sn_{0.6}Te$, a composition range which includes the proposed band crossing. The measurements on PbTe were done at temperatures between 4.2 and 300 K. Most measurements in the alloys were made at 77 K. In six alloy samples, studies were made of the temperature dependence of the Knight shift in the vicinity of the proposed band crossing. The resonances of Sn^{119} and Te^{125} were also studied in the alloy samples, and the Te^{125} resonance was measured in PbTe. As will be discussed below, the Sn^{119} data proved extremely valuable in confirming the identification of the valence- and conduction-band symmetries. The Te^{125} data, however, proved to be of little value, primarily because the extremely weak hyperfine couplings made the Knight shift difficult to observe. For that reason, no formal report of the Te^{125} results will be made here. The interested reader can obtain full documentation of those results from the authors' theses.[1,2]

II. EXPERIMENTAL METHODS

A. Sample Preparation and Characterization

The carrier concentrations of PbTe and $Pb_{1-x}Sn_xTe$ can be changed over wide limits by annealing in either tellurium-rich or metal-rich atmospheres. Since the details of the preparation of our samples have been published elsewhere,[1,2,19] only a general description of the methods used and a summary of the results will be presented here.

Starting materials for the samples were obtained from Bell and Howell and from Texas Instruments. The as-received ingots were generally characterized as "nearly single crystal," but since they were ultimately to be powdered for NMR measurements, no detailed structural examinations were made.

Compositional analyses of the alloy ingots were supplied by Bell and Howell for their materials based on the application of Vegard's law to x-ray powder measurements. Wet chemical analyses of the $x = 0.4$ and $x = 0.5$ ingots agree with Bell and Howell's specifications to within 1%. The $x = 0.17$ samples, obtained from Texas Instruments, were analyzed by the supplier with an estimated precision of 0.1%. In all cases, compositional variations within a slice from any ingot were estimated to be less than 0.5% in the Bell and Howell samples, and less than 0.1% in the Texas Instrument samples.

Slices of the starting-material ingots designated for use as NMR samples were annealed in quartz ampoules together with two bars which were used for characterizing the samples after the anneal. The low-field Hall coefficient and resistivity, measured at 100 Hz at both room and nitrogen tempera-

TABLE I. Summary of PbTe and $Pb_{1-x}Sn_xTe$ NMR samples.

Composition	Type	No. of Samples	Carrier concentration (cm^{-3}) Min	Max
PbTe	p	13	1.0×10^{17}	9.9×10^{18}
	Compensated	1	not known	
	n	6	1.2×10^{17}	1.5×10^{18}
$Pb_{0.83}Sn_{0.17}Te$	p	5	5.0×10^{17}	4.7×10^{19}
	n	1	3.4×10^{16}	...
$Pb_{0.7}Sn_{0.3}Te$	p	5	4.5×10^{18}	1.2×10^{20}
$Pb_{0.65}Sn_{0.35}Te$	p	4	4.5×10^{18}	1.6×10^{20}
$Pb_{0.6}Sn_{0.4}Te$	p	9	3.6×10^{18}	3.6×10^{20}
$Pb_{0.5}Sn_{0.5}Te$	p	11	1.3×10^{19}	5.1×10^{20}
$Pb_{0.4}Sn_{0.6}Te$	p	6	2.7×10^{19}	3.8×10^{20}

tures, were used for this characterization. In all, 61 samples were used in this study, the types and carrier concentrations being summarized in Table I. The carrier concentrations listed in Table I are the reciprocals of the 77-K Hall coefficient. No correction for the Hall-scattering factor was used, partly because the scattering factor is nearly unity for carrier concentrations below 10^{19} cm^{-3}.[20] This approximation and its effect on the results is discussed further in Sec. V. One of the samples listed in Table I, the "compensated" sample, was produced by excessive powdering of what had been an annealed p-type sample. For reasons to be presented below, this sample is believed to have a carrier concentration approximating that of an intrinsic sample. Our model for this reduction in apparent hole concentration, owing to damage-induced levels in the gap, has been discussed in the paper dealing with annealing results.[19]

Once the slices had been annealed and characterized, the final NMR samples were prepared by carefully cutting the slices into coarse powders (~200 μm). It was found that powdering damage of the type that produced the compensated sample could be avoided by cleaving the PbTe samples with a razor blade. This precaution was also followed with the alloy samples, even though no evidence of powdering damage was ever observed.

B. NMR Methods

All NMR measurements were steady-state absorption measurements, using a marginal oscillator of our own design[21] and a 12-in. Varian electromagnet. Signal averaging of repetitive scans was used to combat drifts. Care was taken to avoid saturation of the NMR lines, and the symmetry of the observed lines indicated that the skin-effect admixture of χ' into the absorption signal was not serious. The magnetoresistance of the samples produced a sloping base line which was subtracted out before locating the line centers.

The data were taken with the marginal-oscillator frequency near 10 MHz, monitored with a frequency counter, while the external field was measured with a self-locked proton gaussmeter.[22] Because the gaussmeter could track the swept field, all backlash and time delays in the field sweep were accounted for. All resonance data were scaled to an equivalent external field corresponding to a resonance-line center at precisely 10 MHz.

The temperature-control system used for measurements above 77 K was of conventional design, with the sample and coil contained within a heated can, this can being thermally insulated from a surrounding bath of liquid nitrogen. The sample temperature was measured with a copper-constantan thermocouple attached to the sample can. Offsets errors between the actual sample temperature and the can temperature were eliminated using nuclear-quadrupole-resonance thermometry[23] based on $KClO_3$, a technique which is remarkably useful for NMR cryostat calibration. The system used for measurements below 77 K was similar, except that an exchange gas in contact with a helium reservoir was used for cooling.

III. EXPERIMENTAL RESULTS

A. Knight Shifts and Chemical Shifts

In a semiconductor one is able to separate the chemical shift from the Knight shift with great precision. The Knight shift refers specifically to the shift in resonance field (at constant frequency) produced by the free carriers, while the chemical shift refers to the shift in resonance field produced by all normally filled states, i.e., filled core states, a filled valence band, and an empty conduction band. The two-step procedure for separating the chemical and Knight shifts is outlined below.

The variation of resonance field with carrier

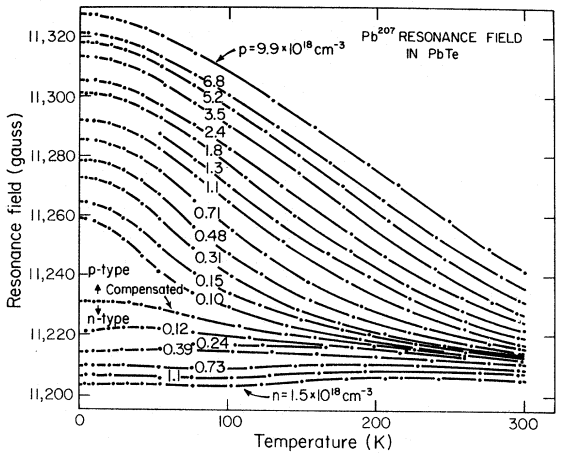

FIG. 1. Pb^{207} resonance field in PbTe at 10 MHz as a function of carrier concentration and temperature.

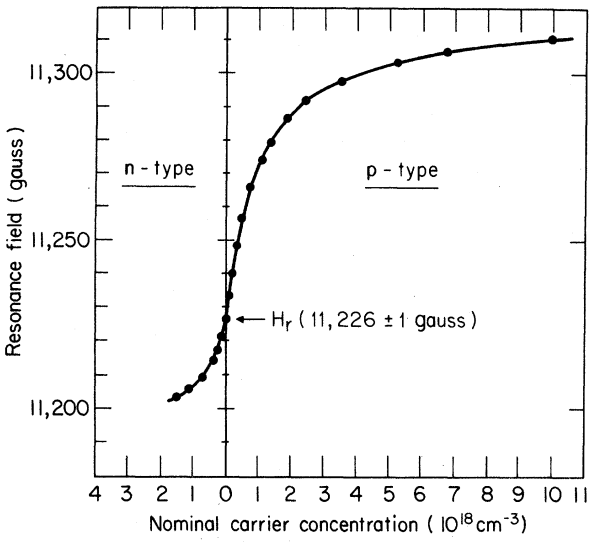

FIG. 2. Pb^{207} resonance field in PbTe at 10 MHz and 77 K as a function of carrier concentration. The reference field H_r is found by interpolation to zero carriers. The datum at zero carriers is from the "compensated" sample.

concentration is used to determine the reference field H_r, the field at which resonance would occur in a sample with no free carriers. The Knight and chemical shifts are then obtained as follows:

$$\text{Knight shift:} \quad (H_r - H_s)/H_s \,, \tag{1}$$

$$\text{chemical shift:} \quad (H_r - H_\mu)/H_r \,, \tag{2}$$

where H_s is the resonance field in the actual sample, and H_μ is the resonance field at the same frequency for the bare nucleus. Equations (1) and (2) incorporate the generally used (and often confusing) sign conventions for these shifts. A positive Knight shift is paramagnetic, requiring an external field H_s smaller than H_r to produce resonance at fixed frequency. A positive chemical shift, however, is diamagnetic, requiring an external field H_r larger than H_μ to produce resonance in a carrier-free sample at constant frequency.

B. NMR in PbTe

The variation of the 10-MHz resonance field of Pb^{207} in PbTe with carrier concentration and temperature is shown in Fig. 1. The temperature range covered by these data is 5–300 K. The previously reported data of Weinberg and Callaway[12] lie approximately on the curve corresponding to a p-type sample with a carrier concentration of 7.1×10^{17} cm^{-3}, in spite of their claim that the carrier concentration of their sample was 1.5×10^{18} cm^{-3}. Since Weinberg and Callaway heated their sample to temperatures as high as 450 K in making their measurements, it is highly probable that they annealed their sample to a lower carrier concentration during their experiment.[15]

The first step in extracting the Knight shift from the data of Fig. 1 is to determine the temperature dependence of the reference field H_r. Figure 2, which shows the carrier concentration dependence of the Pb^{207} resonance field at 77 K, illustrates how H_r can be found by simple graphical interpolation. Plots of this kind were made at a set of temperatures, the resulting reference fields together with the data from the "compensated" sample being shown in Fig. 3. The agreement between the compensated sample and the interpolated reference field is within 1 G at all temperatures. It is this fact which is the basis of our claim of damage compensation in this sample.

The chemical shift at any temperature [Eq. (2)] can be determined from Fig. 3 using the value of the nuclear moment of Pb^{207} from atomic-beam experiments.[24,25] For the moment $\mu(Pb^{207}) = 0.527235\mu_N$, the 10-MHz resonance field H_μ is 11460 G. Thus the Pb^{207} reference field in PbTe corresponds to a paramagnetic chemical shift which increases from a magnitude of 1.99% at 5 K to 2.16% at 300 K. This is a very large chemical shift compared to shifts observed for other nuclei, but it is about the same magnitude as the shifts seen in other lead compounds. The 10-MHz resonance field for Pb^{207} in lead nitrate, for example, is 11267 G, corresponding to a paramagnetic shift of 1.68%. These Pb^{207} chemical shifts are nearly an order of magnitude larger than the chemical shifts in mercury compounds, which were until recently considered to have the largest known chemical shifts.[24] It is likely that relativistic contributions to the Van Vleck orbital paramagnetism play a role here. The spin-orbit mixing

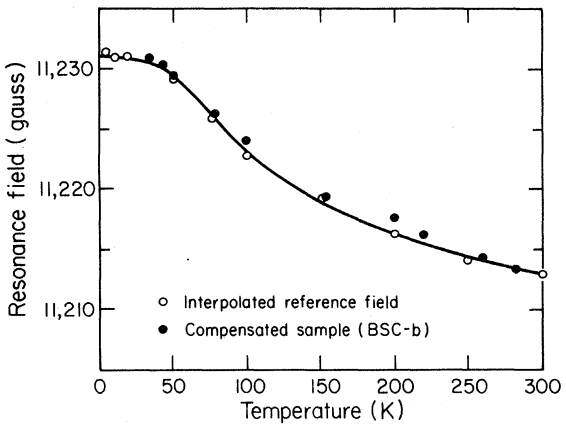

FIG. 3. Temperature dependence of the Pb^{207} reference field in PbTe at 10 MHz. The reference field at 5 K corresponds to a paramagnetic chemical shift of 1.99% relative to the bare Pb^{207} nucleus.

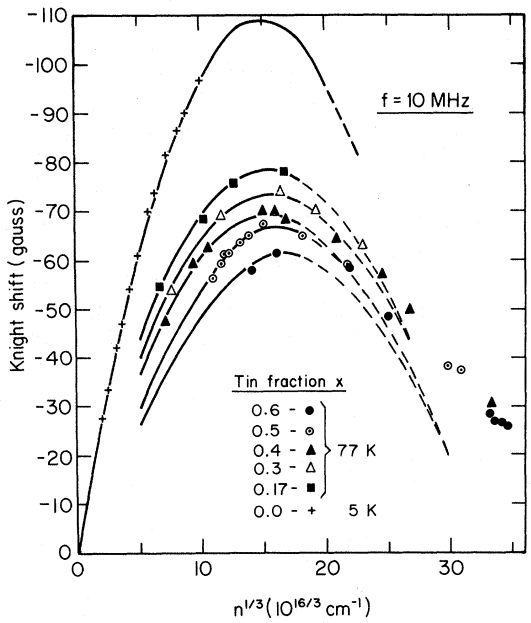

FIG. 4. Carrier concentration dependence of the Pb^{207} Knight shift in PbTe at 5 K and $Pb_{1-x}Sn_xTe$ at 77 K plotted as a function of $n^{1/3}$. The solid curves and the dashed extensions are calculated from the theory.

permits matrix elements of the orbital angular momentum operator between levels which would not contribute significantly to the paramagnetism of the valence band in the absence of spin-orbit mixing. Thus, as the atomic number and spin-orbit mixing increase, corresponding increases in the paramagnetic chemical shift occur.

The Knight shift is obtained from the data of Fig. 1 by combining it with the reference field data of Fig. 3 and using Eq. (1). For example, the Knight shift at 5 K in n-type material is positive, and has a magnitude of 0.2% at 1.5×10^{18} cm^{-3}, while the Knight shift in p-type material is negative, having a magnitude of 0.85% at 9.9×10^{18} cm^{-3}. The signs of these Knight shifts indicate immediately the positive sign of the conduction-band g factor and the negative sign of the valence-band g factor.[15] Furthermore, these Knight shift magnitudes are extremely large for a semiconductor, being nearly as large as metallic Knight shifts. While part of this abnormally large Knight shift can be ascribed to the g factors of the carriers, we shall see that large hyperfine couplings are present as well.

The variation of Pb^{207} Knight shift with carrier concentration at 5 K is shown in Fig. 4 along with corresponding data on the alloys taken at 77 K (see below). The $n^{1/3}$ abscissa is chosen for this plot (n is carrier concentration) because the theory of the Knight shift in semiconductors predicts a linear variation with $n^{1/3}$ in the limit of low temperatures and low carrier concentrations.[14,15] Indeed, the low-concentration data in Fig. 4 are accurately linear, extrapolating from either n type or p type to a reference field of 11 231 G.

We should note in passing that a theory based on parabolic bands would predict $n^{1/3}$ behavior for the Knight shift at all carrier concentrations. Thus, the departures from $n^{1/3}$ behavior observed in PbTe can be used to provide valuable information on the nonparabolicity of the band structures.

As the temperature is increased above 5 K, the Pb^{207} Knight shifts in both n- and p-type material decrease, gradually below 100 K, more rapidly above (refer to Fig. 1). Some of this temperature dependence can be explained entirely on the basis of the change from degenerate to nondegenerate statistics and the concommitant motion of the Fermi level out of the band. However, we shall show that there is an additional temperature dependence which cannot be accounted for in this way.

C. NMR in $Pb_{1-x}Sn_xTe$

The carrier concentration dependence of the Pb^{207} Knight shift in $Pb_{1-x}Sn_xTe$ at 77 K is shown in Fig. 4 plotted as a function of composition assuming a constant reference field of 11 226 G at 77 K. All of the samples are p type except for the one n-type $x = 0.17$ sample shown. Corresponding data for the Sn^{119} Knight shifts are shown in Fig. 5, and are plotted assuming that the reference field is 6308 G at 77 K. The reason for these choices of reference field are discussed below.

In the alloys, it is not possible to make n-type

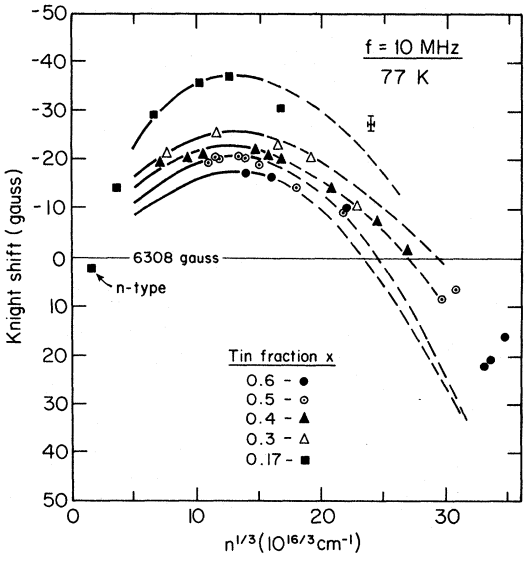

FIG. 5. Carrier concentration dependence of the Sn^{119} Knight shift in $Pb_{1-x}Sn_xTe$ at 77 K and 10 MHz, plotted as a function of $n^{1/3}$.

material in compositions with $x > 0.25$, and it becomes increasingly difficult to make low-carrier-concentration p-type material as the tin fraction increases. Therefore, a direct measurement of the reference field is not possible for most of the alloy compositions. Instead, one must rely on measurements of the reference field for $x < 0.25$. The single n-type sample with $x = 0.17$ provides an important indication that the reference field is independent of composition. The n-type $x = 0.17$ sample has a carrier concentration of 3.4×10^{16} cm^{-3}. The Pb^{207} resonance in this sample occurs at 11 221 G, almost exactly where the resonance in a PbTe sample of this carrier concentration would occur at 77 K. Therefore, the Pb^{207} reference field at $x = 0.17$ is within about 1 G (the experimental precision) of the reference field in PbTe. This is a reasonable result if one recalls that tin and lead have identical electronegativities (1.8 on Pauling's scale), and that there is a strong correlation between electronegativity and chemical shift.[26] On the basis of this result and these arguments, we have assumed that the Pb^{207} reference field is independent of x for all alloy compositions, an assumption which is likely to be no more than a few gauss in error over the entire range of compositions studied.

The Sn^{119} reference field in the alloys (6308 G) is determined in a similar way. The Sn^{119} resonance in the n-type $x = 0.17$ sample occurs at 6306.2 G. By noting the difference in magnitude between the Pb^{207} and Sn^{119} Knight shifts in Figs. 4 and 5 (by comparing, for example, the relative change in resonance fields for the same change in carrier concentration), and by noting that the Pb^{207} Knight shift is estimated at 5 G for this sample, the Sn^{119} Knight shift is estimated at 1.8 G. On this basis, the reference field of 6308 G is found, and presumed constant for all alloys, an assumption which should be valid to within a few gauss over the entire composition range.

The most remarkable feature illustrated in Figs. 4 and 5 is that the Knight shift goes through a maximum as a function of carrier concentration, an unexpected variation that is unique to $Pb_xSn_{1-x}Te$. We now understand the origin of this maximum in the context of $\vec{k} \cdot \vec{p}$ theory.[3] It arises from the far-band and free-electron contributions to the $\vec{k} \cdot \vec{p}$ energies and eigenfunctions, producing a Knight shift term opposite in sign to the principal two-band contribution. At high carrier concentrations, the far-band terms dominate, accounting for the maximum.

Another interesting feature of the data is the general variation of the Knight shift with composition. Naively, one might expect the Knight shift to get larger as the composition changes from pure PbTe towards the narrower-band-gap materials ($x = 0.4$ is expected to have zero gap at about 80 K), because the g factors should get very large when the gap is small. Instead, there is a monotonic decrease in Knight shift with increasing tin fraction. This effect is ascribed to an explicit dependence of the hyperfine coupling constants on composition, as discussed in more detail later.

Figure 6 shows the Pb^{207} Knight shift in six alloy samples as functions of temperature in the vicinity of the band crossings expected for the various compositions. The temperatures at which $x = 0.35$, 0.40, and 0.50 are expected to have band crossings are

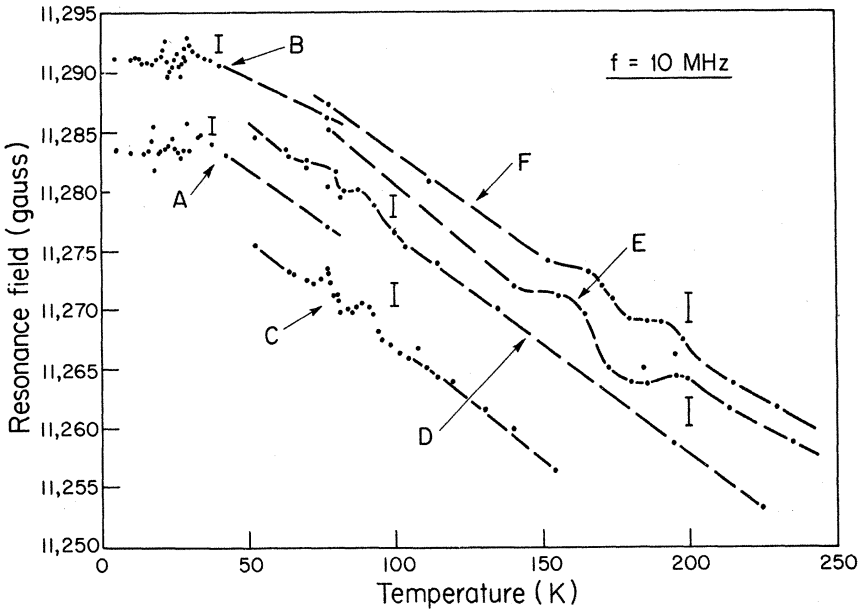

FIG. 6. Temperature dependence of the Pb^{207} Knight shift in six alloy samples in the vicinity of their respective band inversions: (a) $x = 0.35$, $p = 4.5 \times 10^{18}$ cm^{-3}; (b) $x = 0.35$, $p = 9.2 \times 10^{18}$ cm^{-3}; (c) $x = 0.4$, $p = 3.7 \times 10^{18}$ cm^{-3}; (d) $x = 0.4$, $p = 8.2 \times 10^{18}$ cm^{-3}; (e) $x = 0.5$, $p = 1.6 \times 10^{19}$ cm^{-3}; (f) $x = 0.5$, $p = 1.7 \times 10^{19}$ cm^{-3}. The observed structure cannot be explained on the basis of Landau levels.

25, 80, and 180 K respectively. There is apparent structure, although poorly resolved, in the temperature dependence in each sample within a temperature region about the band crossing. As with PbTe, the general decrease of the Knight shift with increasing temperature is easily understood, but the structure in the curves remains unexplained at the present time, even using a model which explicitly takes account of Landau levels.

D. NMR Linewidths

It was observed that the NMR linewidths depend in a regular way on temperature, composition, and carrier concentration. Generally, linewidths increase with increasing carrier concentration and increasing tin fraction, and decrease with increasing temperature. In PbTe, the Pb^{207} linewidth at 5 K increased from 2.5 G at low carrier concentrations to 6 G at 10^{19} cm^{-3}, the corresponding range at 300 K being 2.5–4 G. In the alloys, the Pb^{207} linewidths were broader than in pure PbTe, the range at 77 K being from 8 to about 40 G, a typical figure being 20 G. The typical linewidth for Sn^{119} resonances was 10 G.

IV. THEORY

There are two kinds of information one can hope to learn from the NMR experiments reported above. With the reasonable assumption that for constant x the variation of hyperfine couplings with carrier concentration can be accurately modeled in terms of $\vec{k}\cdot\vec{p}$ admixtures of valence- and conduction-band wave functions, one can extract from the variation of the Knight shift with carrier concentration quantitative information about the structure of the valence and conduction bands. On the other hand, once a band model is developed consistent both with the observed variation of the Knight shift with carrier concentration and with other available data on effective masses and g factors, then the overall magnitude of the Knight shift and its variation with composition provide measurements of the strength and composition dependence of the hyperfine couplings themselves.

An important premise in our use of the $\vec{k}\cdot\vec{p}$ approach to a band model is the presumption that the $Pb_{1-x}Sn_xTe$ alloys can be considered as a single system, with the matrix elements of momentum not being strong functions of composition. Accordingly, one might hope to be able to combine experimental data from different compositions and obtain a single self-consistent set of matrix elements for this system. We will show that this expectation is realized to a great extent in these materials.

A. Band Model

The band model used as a basis for the analysis of the NMR data is reported in complete detail in the accompanying paper.[3] Briefly, the model is a six-band $\vec{k}\cdot\vec{p}$ model, in which couplings between the valence band and far bands and between the conduction band and far bands are treated in perturbation theory, while the direct couplings between the conduction and valence bands are treated exactly. The discussion to follow will deal with the hyperfine couplings, the one subject not treated extensively in the theory paper.

B. Hyperfine Interactions

In order to calculate the effect of a hyperfine coupling between a nucleus and a carrier on the nuclear resonance frequency, one must evaluate for each occupied carrier state the diagonal matrix element of an effective field operator derived from the hyperfine Hamiltonian. Using the notation of the accompanying paper,[3] we write a one-electron state in the form

$$\Psi^{n,k_B,k_y}_{m,\sigma}(\vec{r}) = \sum_{m',\sigma'} C^{n,k_B,k_y}_{m,\sigma,m',\sigma'}(\vec{r})\,\Psi^{T}_{m',\sigma'}(\vec{r}), \qquad (3)$$

where $\Psi^{T}_{m',\sigma'}$ is a linear combination of the four band-edge Bloch functions (spin up and spin down for both L_6^+ and L_6^-), and $C(\vec{r})$ is a harmonic-oscillator amplitude function characteristic of Landau levels. The quantum numbers are defined as follows: m is a band index (L_6^+ or L_6^-), σ is a spin index, k_B is the wave vector in the direction of the magnetic field (the field is chosen to lie in the x-z plane, with z along $\langle 111\rangle$), k_y is the wave vector in the y direction, and n is the Landau level index. The specific linear combination of Bloch states in $\Psi^{T}_{m',\sigma'}$ depends on the orientation of the external field, and the order of the Hermite polynomial appearing in $C(\vec{r})$ depends on the five quantum numbers n, m, σ, m', and σ'.

There are several kinds of hyperfine interactions between a carrier and a nucleus which can give rise to a Knight shift. In roughly decreasing order of importance, these are, (i) the contact interaction, (ii) the orbital hyperfine interaction, (iii) core polarization, and (iv) the spin-dipole and spin-other-orbit hyperfine interactions. The contact hyperfine interaction is nonzero for s states. For non-s states the leading term is the orbital hyperfine interaction, particularly in the lead salts where the large-spin-orbit couplings gives rise to substantial unquenching of the local orbital moment. There is also a spatially distributed orbital moment associated with the orbital quantization into Landau levels. Yafet[27] has shown, however, that this distributed moment is very weakly coupled to any single nuclear moment, and thus produces a negligibly small contribution to the Knight shift. We shall be concerned only with the leading interactions, (i) and (ii) above.

For either of the hyperfine interactions, one can write down an effective-field operator. If the

oscillator amplitude $C(\vec{r})$ is reasonably constant over the dimensions of a unit cell, then the diagonal matrix element of such an operator Q between states $\Psi_{m,\sigma}^{n,k_B,k_y}$ can be represented approximately as

$$\langle\Psi \mid Q \mid \Psi\rangle \cong \left(\int_{\text{unit cell}} d\tau\, \Psi^{T\dagger} Q \Psi^{T}\right) \times \sum_{\text{lattice}} C^{\dagger}(\vec{r}_i) C(\vec{r}_i)\,, \quad (4)$$

where the integral over a unit cell has been factored out, leaving what amounts to a sampled normalization integral for $C(\vec{r})$. In our case, the variation in amplitude of $C(\vec{r})$ occurs on a scale much larger than a unit cell. Therefore, it is reasonable to focus attention on the cell-periodic part of the matrix element $\langle\Psi^T \mid Q \mid \Psi^T\rangle$ which is in turn linearly related to the matrix elements of Q between the band-edge Bloch states. In the paragraphs to follow we shall examine in detail the symmetry of band-edge states and the parametrization of the corresponding matrix elements of the hyperfine operators.

We will adopt the notation of Mitchell and Wallis (MW)[28] in describing the symmetry of the Bloch states. The L-point valence-band states of lead telluride denoted by L_6^+ are written as

$$L_6^+\alpha = -i\cos\theta^+ R\uparrow - \sin\theta^+ S_+\downarrow\,,$$
$$L_6^+\beta = i\cos\theta^+ R\downarrow + \sin\theta^+ S_-\uparrow\,, \quad (5)$$

where the spatial function R and S transform about the metal nucleus like atomic s states and d states, respectively, and where $\cos\theta^+$ and $\sin\theta^+$ describe the spin-orbit mixing of these wave functions. The spin labels $\uparrow$, $\downarrow$ refer to a basis set diagonal in s_z for z along $\langle 111\rangle$. Notice that the wave functions are not pure spin states. Band calculations[4] indicate that this L_6^+ level is strongly dominated by the R component. As will be discussed in Sec. V A, the identification of the L_6^+ level as the valence band of PbTe is strongly supported by the Knight shift experiments.

The L-point L_6^- states in the MW notation are

$$L_6^-\alpha = \cos\theta^- Z\uparrow - \sin\theta^- X_+\downarrow\,,$$
$$L_6^-\beta = \cos\theta^- Z\downarrow + \sin\theta^- X_-\uparrow\,, \quad (6)$$

where Z and $X_\pm$ represent spatial wave functions which transform like atomic p states about the metal nucleus. The spin-orbit mixing (described by $\cos\theta^-$ and $\sin\theta^-$) is responsible for the fact that the states are not pure spin states and, as shown below, also serves to unquench the orbital angular momentum of the L_6^- states.

As shown in the accompanying theory paper,[3] the effective-field operator for the contact interaction and orbital contributions to the Knight shift is proportional to the diagonal matrix elements of the following operator:

$$Q = \tfrac{8}{3}\pi s_B\,\delta(\vec{r}) + l_B/r^3\,, \quad (7)$$

where s_B and l_B are the components of electron spin and orbital angular momentum in the direction of the applied field, and $\vec{r}$ is the electron coordinate measured from the nuclear position. In the coordinate system of a single L-point valley with z along $\langle 111\rangle$, it is necessary to know the matrix elements of both the x and z components of $\vec{s}\,\delta(\vec{r})$ and $\vec{l}/r^3$ in order to calculate the projections along an arbitrary field direction.

For the L_6^+ levels of Eq. (5), in which the R term represents 95% of the total wave function[4,5] the contact interaction dominates the Knight shift. The matrix elements of interest are

$$\langle L_6^+\alpha \mid s_z\delta(\vec{r}) \mid L_6^+\alpha\rangle = -\langle\beta \mid \mid \beta\rangle = \tfrac{1}{2}\cos^2\theta^+\langle R \mid \delta(\vec{r}) \mid R\rangle\Omega \quad (8)$$

and

$$\langle L_6^+\alpha \mid s_x\delta(\vec{r}) \mid L_6^+\beta\rangle = -\tfrac{1}{2}\cos^2\theta^+\langle R \mid \delta(\vec{r}) \mid R\rangle\Omega\,,$$

where Ω is the unit-cell volume chosen for normalization. The equality (in magnitude) of the s_x and s_z matrix elements reflects the spatial isotropy of the contact interaction. Therefore, the magnitude of the contact interaction part of the L_6^+ hyperfine interaction can be accurately represented with a scalar defined as

$$A_c = \tfrac{8}{3}\pi\cos^2\theta^+\langle R \mid \delta(\vec{r}) \mid R\rangle\Omega\,. \quad (9)$$

We shall assume that the entire hyperfine interaction of the L_6^+ level can be represented by this contact interaction matrix element. In doing so, we are neglecting an orbital contribution from the d-like part of the L_6^+ state and we are neglecting core polarization and other Knight shift contributions. The neglect of the orbital term is fully justified by the fact that only 5% of the L_6^+ wave function is non-s-like, and that these higher angular momentum states normally are coupled less strongly to the nucleus than are s states. The core polarization could constitute a modest fraction of the total Knight shift,[29–31] but since core polarization involves contact interaction couplings to core s states, the presence of a core polarization component cannot be distinguished from the direct contact interaction with the L_6^+ level. Thus the parameter A_c can be used to represent parametrically both the direct and core polarization contact interactions.

For the L_6^- levels [Eq. (6)] which transform like p states about the Pb (or Sn) nucleus, the contact interaction is zero. The matrix elements of the orbital interaction are

$$\langle L_6^- \alpha \,|\, l_z/r^3 \,|\, L_6^- \alpha\rangle = -\langle \beta \,|\, |\beta\rangle = \sin^2\theta^- \langle X_+ \,|\, 1/r^3 \,|\, X_+\rangle \Omega\,, \quad (10)$$

$$\langle L_6^- \alpha \,|\, l_x/r^3 \,|\, L_6^- \beta\rangle = \sqrt{2}\, \sin\theta^- \cos\theta^- \langle X_+ \,|\, 1/r^3 \,|X_+\rangle \Omega\,,$$

where the transformation properties of the Z and X_+ components of the L_6^- states have been used to reduce the matrix elements to simplest form. In the limit of strong spin-orbit coupling ($\cos\theta^- = 1/\sqrt{3}$), the orbital interaction of L_6^- would be spatially isotropic, just as the contact interaction was for L_6^+. Band calculations,[4,5,7] however, estimate the magnitude of $\cos\theta^-$ to be near the selected value[7] of 0.87, an intermediate coupling case. Faced with extremely sparse data on n-type material, and that primarily at relatively low carrier concentrations, it was decided to model the L_6^- orbital interaction as isotropic, recognizing that this will restrict our ability to relate the single orbital hyperfine constant obtained from experiment to the matrix element $\langle X_+|1/r^3|X_+\rangle$. The parameter corresponding to A_c for the orbital case is denoted by A_0. It can be approximated by the orientational average of $\langle L_6^-\alpha|l_z/r^3|L_6^-\alpha\rangle$ and $\langle L_6^-\alpha|l_x/r^3|L_6^-\beta\rangle$; that is,

$$A_0 \cong (\tfrac{1}{3}\sin^2\theta^- + \tfrac{2}{3}\sqrt{2}\sin\theta^-\cos\theta^-)\langle X_+|1/r^3|X_+\rangle\Omega\,. \quad (11)$$

It should be noted that the principal role played by the L_6^- interaction in p-type material is that of a small correction to the total Knight shift. Thus approximations to the L_6^- coupling are far more permissible than for the L_6^+ coupling. If a source of experimental data develops from which the anisotropy of the L_6^- hyperfine coupling could be determined, an anisotropic orbital interaction could be included in the theory.

Throughout the above discussion, it has been implicitly assumed that replacing a Pb atom with a Sn atom makes only a small perturbation on the band structure, the principal effect being a shift in the one-electron L_6^+ energy. When dealing with hyperfine interactions, however, which are dominated by extremely local features of the wave function, it is necessary to distinguish between couplings to Pb^{207} nuclei and to Sn^{119} nuclei. Accordingly, we shall define experimentally a pair of hyperfine constants A_c and A_0 for each nuclear species, denoting them with superscripts Pb and Sn, and examine carefully whether the variation in A_c and A_0 between Pb site and Sn sites and their dependence on composition can be interpreted in a way consistent with this energy-band picture of the alloy system.

V. INTERPRETATION

A. Low-Temperature Band Structure

In this section we shall present the results of a fit of the Pb^{207} Knight shift data, the Sn^{119} Knight shift data, and other available data on energy gaps, effective masses, and g factors with the parametrized $\vec{k}\cdot\vec{p}$ theory described earlier. The result of this fitting procedure is a set of $\vec{k}\cdot\vec{p}$ parameters and hyperfine coupling constants which adequately account, in a self-consistent way, for all data in the temperature region below about 100 K, excepting only the Knight shift anomalies observed in the band inversion region (see Sec. V D below).

1. Energy Gap Variation

Data on the variation of the principal energy gap E_G were compiled from the literature.[9,32–43] The results of this survey can be summarized as follows: At constant temperature, the data are well represented by Smith's formula[9] based on deformation potentials:

$$|E_G(x,T)| = |E_G(0,\ T) - 0.543x + 0.02x^2|\ \text{eV}\,, \quad (12)$$

where $E_G(0,\ T)$ represents the temperature dependence of the PbTe energy gap. This gap, based on the available data in PbTe and in the homologous materials PbS and PbSe,[44] is effectively constant up to a temperature of about 50 K, beyond which the gap increases with a temperature coefficient of 4.85×10^{-4} eV/K. The value of $E_G(0,\ 0)$ is 0.187 eV. In the analysis described below the energy gap appropriate to each composition and temperature was obtained from the relations above, and used in all calculations.

2. Determination of $\vec{k}\cdot\vec{p}$ Parameters

It is assumed at the outset that for each composition x, the band structure can be represented in terms of nine $\vec{k}\cdot\vec{p}$ parameters: the principal gap E_G, the direct momentum matrix elements v_t and v_l, and six terms of the form $|v_{fb}|^2/E_{fb}$, where v_{fb} is a matrix element to a far band and E_{fb} is the corresponding energy gap (see Fig. 1 of Ref. 3). The specific methods used to calculate each experimental quantity in terms of these $\vec{k}\cdot\vec{p}$ parameters have been described elsewhere.[3]

The determination of the $\vec{k}\cdot\vec{p}$ parameters from the data proceeded in several iterative steps. First, low-temperature data on band edge masses and g factors were compiled for PbTe. The data gleaned from the literature imposed a preliminary set of constraints on possible self-consistent sets of values of the various $\vec{k}\cdot\vec{p}$ parameters. Next, the variation of the PbTe Knight shift with carrier concentration was analyzed, using two additional parameters A_c^{Pb} and A_0^{Pb} to characterize the band-edge L_6^+ and L_6^- hyperfine constants. This calculation explicitly included the admixture of L_6^+ and L_6^- wave functions in states away from the band edge. The result of this analysis was a much tighter set of constraints on possible values of the $\vec{k}\cdot\vec{p}$ parameters as well as experimentally determined values

for the hyperfine parameters. Finally, as a check, calculations were made for the effective masses and g factors away from the band edge, as obtained in Shubnikov–de Haas and other magneto-oscillatory experiments. It was found that calculated values using the $\vec{k}\cdot\vec{p}$ parameters based only on band-edge masses, g factors, and the Knight shift agreed with other data to within experimental error.

In the calculations of the Knight shift described above, it was necessary to ascribe opposite algebraic signs to the two principal momentum matrix elements v_l and v_t. Confirmation of the necessity of this assignment of relative signs is obtained from our analysis of the NMR linewidth (see Sec. V A 3 below). In terms of the spin-orbit mixing parameters $\cos\theta^{\pm}$ and $\sin\theta^{\pm}$, this means that $\cos\theta^{+}$, $\sin\theta^{+}$, and $\cos\theta^{-}$ can be chosen as positive, but that $\sin\theta^{-}$ must be taken as negative, in direct disagreement with the theoretical result of Bernick and Kleinman.[7]

Once the low-temperature parameters for PbTe were determined, analysis of the remaining data was made with minimal perturbations of the PbTe results. Considering first the low-temperature data on the alloys, the experimentally observed variation of E_G with x and T was used together with available data on masses and g factors to determine what variation, if any, was needed in the $\vec{k}\cdot\vec{p}$ parameters to account for observed results. The position of the maximum in the Knight shift versus carrier concentration was particularly useful here in establishing the relative sizes of far-band and two-band $\vec{k}\cdot\vec{p}$ parameters. It was found that by including the explicit variation of the principal gap, almost no other variation in any of the $\vec{k}\cdot\vec{p}$ parameters was required to obtain satisfactory agreement with published data on effective masses and g factors. It must be noted, however, that the data on these quantities is limited to compositions with $x < 0.3$. At the same time, it was found that the only satisfactory way to account for the observed variation of the Knight shift with carrier concentration at each composition measured was to ascribe an explicit composition dependence to the hyperfine couplings. This result, that the hyperfine couplings are more sensitive to compositional changes than are the momentum matrix elements, is one of the surprising outcomes of this analysis.

The temperature dependence of the PbTe Knight shift was calculated at each carrier concentration using the $\vec{k}\cdot\vec{p}$ parameters obtained for the low-temperature band structure, but using energy gap and the Fermi factor appropriate to the elevated temperature. For temperatures less than about 100 K, this method was totally satisfactory in accounting for the observed variation of Knight shifts (excepting the anomalies observed near the band crossings in the alloys). Above 100 K, however, where the PbTe data show a marked decrease in Knight shift with increasing temperature, it was necessary to ascribe an "effective temperature dependence" to the principal momentum matrix elements, a "forced fit" to experiment not to be generally recommended.

Table II contains our final set of $\vec{k}\cdot\vec{p}$ parameters and hyperfine constants, displayed as functions of composition. The complete data base used to develop these parameters together with corresponding calculated quantities is shown in Table III. Finally, the calculated variation of the Pb^{207} and Sn^{119} Knight shifts with carrier concentration are shown as the solid curves in Figs. 4 and 5. Perusual of Table III and the figures show that the agreement between theory and experiment is excellent and in all but a few cases, within stated experimental error. Thus the parameters of Table II, at least in an empirical sense, account very well for all observed features of the low-temperature band structure of these systems.

We should note that the "minimum perturbation" of the PbTe parameters adopted to carry out the fit to the alloy data necessitated no change whatsoever in the principal matrix elements of momentum v_l and v_t. Furthermore, the modest variations in the far-band parameters shown in the table are entirely consistent with the possible variations of far-band energy gaps with composition. Thus in a very real sense, the parameters in Table II constitute nearly a single set of parameters which characterize the alloy system over the entire composition range examined.

The precision with which the parameters in Table II are known can be described as follows: Each experimental datum, whether Knight shift measurement or a measurement of a feature of the energy bands, provides one constraint on the possible values of a subset of the $\vec{k}\cdot\vec{p}$ parameters. When all the data are taken together, the intersection of all the individual constraints place rather tight restrictions on the relative magnitudes of the parameters. However, the set of parameters in Table II is certainly not unique. Many such internally self-consistent sets may be obtained by varying the two-band matrix elements by as much as 10%, provided one makes corresponding adjustments (up to 20%) in the far-band parameters. It must be emphasized, however, that the relations between the parameters within any set are much more tightly constrained than this 10% figure. The hyperfine constraints, which are derived principally from the slope of the Knight shift versus carrier concentration at low carrier concentration, could vary by as much as 25% in response to a 10% variation in the two-band matrix elements,

this 25% figure being our estimate of the experimental uncertainty with which these quantities can be said to be determined from this experiment.

Within the error limits stated above, the neglect of the departure of the Hall-scattering factor from unity (Sec. II A) is believed to be fully justified. Allgaier[20] has determined the scattering factor in p-type PbTe by comparing low-field and high-field Hall coefficients, observing that for carrier concentrations below 10^{19} cm^{-3}, the scattering factor is 0.9 or larger. Values as low as 0.7 and 0.6 are observed at carrier concentrations above 3×10^{19} cm^{-3},[53–55] a region in which the validity of $\vec{k}\cdot\vec{p}$ model itself is questionable. For the region below 3×10^{19} cm^{-3} in which we actually use the $\vec{k}\cdot\vec{p}$ model, the scattering factor can be ignored. Furthermore, the effect of neglecting the scattering factor is to make the nominal carrier concentration a slight overestimate beyond 3×10^{19} cm^{-3}. In Figs. 4 and 5, we have extended the $\vec{k}\cdot\vec{p}$ calculations of the Knight shift into this region (dashed curves). If the data for the higher carrier concentrations were to be replotted with corrected rather than nominal carrier concentrations, the agreement between theory and experiment would actually improve.

3. *Linewidth Studies*

While no systematic study of line shapes was made in this experimental program, several interesting features of the variation of linewidth with carrier type and concentration are worth noting. It was observed that the Pb^{207} linewidth in PbTe at low temperatures increased from about 2.5 G at low carrier concentrations to about 6 G at 10^{19} cm^{-3}. Our $\vec{k}\cdot\vec{p}$ model shows explicitly that the nonellipsoidal energy surfaces produced by the far-band matrix elements will give rise to an orientation dependence of the Knight shift.[2,3] In a powder, this orientation dependence serves as a mechanism for line broadening. The more distant the Fermi level from the band edge, the more important are the far-band terms in determining the shape of the constant energy surface, with the result that the Knight shift anisotropy and powder linewidth increase with increasing carrier concentration. Explicit calculations[2] of the Knight shift anisotropy for the choice of $\sin\theta^-$ negative indicate that a line width of about 3 G should be expected for a powder sample at 10^{16} cm^{-3} in p-type lead telluride, increasing to about 6 G at 10^{19} cm^{-3} in good agreement with the data. A choice of $\sin\theta^-$ as positive would result in calculated linewidths twice too large, thus confirming the sign assignment discussed in Sec. V A 2 above.

Because the linewidth in PbTe is largely the result of inhomogeneous broadening (the minimum linewidth observed was 2.5 G), it is not at all surprising that the decrease in Knight shift with increasing temperature should be accompanied by corresponding decrease in linewidth. While no quantitative analysis was made above 50 K, the trend in the data is in general agreement with our expectation.

In the alloys, the linewidths were much larger than calculated estimates based on the Knight shift

TABLE II. Final $\vec{k}\cdot\vec{p}$ parameters and hyperfine constants obtained from an iterative fit to available data. The notation used is that of Ref. 3 (We are using the values $\cos^2\theta^+=0.956$ and $\cos^2\theta^-=0.755$ for the spin-orbit mixing parameters).

Parameter	Tin fraction					
E_G(eV)(T=77 K)	0.00 0.217	0.17 0.125	0.30 0.056	0.40 0.003	0.50[a] −.049	0.60[a] −.101
v_t^2	0.41	0.41	0.41	0.41	0.41	0.41
v_l^2	0.038	0.038	0.038	0.038	0.038	0.038
$\lvert v_{t,+1}\rvert^2/E_{+1}$	5.0	7.0	5.75	5.5	4.5	4.5
$\lvert v_{l,+1}\rvert^2/E_{+1}$	1.7	1.9	1.7	1.7	1.7	1.7
$2\lvert v_{t,+2}\rvert^2/E_{+2}$	6.0	6.0	5.25	5.0	4.0	4.0
$\lvert v_{t,-1}\rvert^2/E_{-1}$	4.6	4.6	4.6	4.6	4.1	3.6
$\lvert v_{l,-1}\rvert^2/E_{-1}$	0.2	0.2	0.2	0.2	0.2	0.2
$2\lvert v_{t,-2}\rvert^2/E_{-2}$	6.0	6.0	6.0	6.0	5.5	5.0
$A_c^{Pb}\times10^{-5}$	1.25	0.78	0.71	0.70	0.71	0.63
$A_0^{Pb}\times10^{-5}$	0.50	0.31	0.28	0.28	0.29	0.25
$A_c^{Sn}\times10^{-5}$		0.83	0.55	0.61	0.85	0.84
$A_0^{Sn}\times10^{-5}$		0.11	0.07	0.08	0.11	0.02

[a]The negative energy gap indicates the SnTe-rich side of the band inversion.

TABLE III. Comparison between experimental data from the literature and corresponding calculated values (in parentheses) based on the model. The principal gap appropriate to the composition and temperature of each experimental point was used in each calculation.

Composition (X)	Carrier concentration (cm^{-3})	Anisotropy (K)	A^{111} $(1/a_B^2)$[a]	Effective mass m_c^{111}/m_0, m_r^{100}/m_0[b]	g factors g_l, g_t, g_{110}, g_{100}, g_{fb}[c]	Comment and Ref.[d]
0.00	Valence band edge	14 ± 2 (11.5)		m_c^{111}: 0.022 ± 0.003 (0.025)	g_l: 51 ± 8 (56)	45
"	Conduction band edge	10 ± 1.5 (10.5)		m_c^{111}: 0.024 ± 0.003 (0.024)	g_l: 45 ± 8 (58)	45
	Band edge			m_r^{100}: 0.022 (0.020)[e]	g_{100}: 29 (34)[e] g_{fb}: 15.9 (16.9)	33
				m_r^{100}: 0.0215 ± 0.0005 (0.0215)[e]		(77 K) 32
				m_r^{100}: 0.0204 ± 0.0005 (0.0200)[e]		32
	Band edge			m_r^{100}: 0.0195 (0.020)[e,f]		(47 K) 34
				m_r^{100}: 0.0233 (0.0227)[e,f]		(97 K) 34
	p 3.0×10^{18}	13 (12)	2.94×10^{4} (3.1×10^{-4})	m_c^{111}: 0.036 ± 0.002 (0.038)	g_l: 32 ± 2 (32.7) g_t: 7 ± 2 (4)	46
	p 3.5×10^{18}		3.85×10^{-4} (3.86×10^{-4})	m_c^{111}: 0.038 ± 0.002 (0.039)	g_l: 30 (31.5) g_t: 10 (3.4)	46
	p 9.2×10^{17}		1.40×10^{-4} (1.41×10^{-4})	m_c^{111}: 0.027 ± 0.003 (0.031)		46
	n 8×10^{16}				g_l: 57.5 ± 2 (57.5) g_t: 15 ± 1 (14.9)	47
					g_{110}: 46 (47.7) g_{100}: 35.5 (35.3)	47
	p 2×10^{17}	12.2 (12.2)		m_c^{111}: 0.03 (0.026)		48
	n 2×10^{17}	9.8 (10)		m_c^{111}: 0.024 (0.025)		48
	n 8.1×10^{17}			m_c^{111}: 0.0245 (0.028)		49
	h 1.7×10^{17}			m_c^{111}: 0.0215 (0.024)		49
0.09	Band edge			m_r^{100}: 0.0151 (0.0154)[e]	g_{100}: 56 (48)[e]	(47 K) 34

TABLE III. *continued*

Composition (X)	Carrier concentration (cm^{-3})	Anisotropy (K)	A^{111} $(1/a_B^2)$[a]	Effective mass m_c^{111}/m_0, m_r^{100}/m_0[b]	g factors g_l, g_t, g_{110}, g_{100}, g_{fb}[c]	Comment and Ref.[d]
0.16	Band edge			m_r^{100}: 0.0187 (0.0184)[e]	g_{100}: 38 (37)[e]	(97 K) 34
0.16	Band edge			m_r^{100}: 0.0122 (0.0118)[e]	g_{100}: 69 (67)[e]	(47 K) 34
0.16	Band edge			m_r^{100}: 0.0151 (0.0150)[e]		(97 K) 34
0.164	n 4.3×10^{16}		2.09×10^{-5} (1.87×10^{-5})	m_c^{111}: 0.014 ± 0.002 (0.016)		50
0.18	Valence band edge			m_c^{111}: 0.014 (0.013)		51
0.185	p 3.1×10^{16}		1.8×10^{-5} (1.46×10^{-5})	m_c^{111}: 0.0120 ± 0.0015 (0.0146)		50
0.186	p 2.6×10^{17}	10.5 (11.6)	6.0×10^{-5} (6.0×10^{-5})	m_c^{111}: 0.016 ± 0.0015 (0.018)		50
0.19	Band edge			m_r^{100}: 0.011 (0.010)[e]	g_{100}: 77 (80) g_{ft}: 15.9 (17.4)	37
0.20	p 1.1×10^{18}	10 ± 2 (12)		m_c^{111}: 0.022 ± 0.003 (0.024)		52
0.21	Band edge			m_r^{100}: 0.01 (0.01)[e]	g_{100}: 84 (84)[e] g_{fb}: 15.7 (17.4)	37
0.216	p 8.5×10^{17}	11.2 ± 0.5 (11.3)	1.34×10^{-4} (1.35×10^{-4})	m_c^{111}: 0.0225 ± 0.0015 (0.0219)	g_{110}: 52 ± 4 (57) g_{100}: 37 ± 3 (41)	50
0.26	Band edge			m_r^{100}: 0.0077 (0.0077)[e]	g_{100}: 112 (112)[e] g_{fb}: 15.9 (16.1)	37
0.27	Band edge			m_r^{100}: 0.0074 (0.0074)[e]	g_{100}: 120 (120)[e] g_{fb}: 15.9 (16.1)	37
0.31	p 2.2×10^{17}	10.5 ± 1.0 (11.1)	5.29×10^{-5} (5.49×10^{-5})	m_c^{111}: 0.014 ± 0.0015 (0.0136)		50
0.315	p 1.8×10^{18}	10.5 ± 0.7 (11.4)	2.04×10^{-4} (2.24×10^{-4})	m_c^{111}: 0.0275 ± 0.002 (0.0273)		50

[a] a_B = Bohr radius

[b] $1/m_r^{100} = 1/m_{L_6^+}^{100} + 1/m_{L_6^-}^{100}$

[c] g_{fb} is the slope of the field dependence of the lowest energy interband transition in magneto-optical experiments.

[d] Data obtained near 4.2 K except as noted.

[e] Obtained by averaging valence- and conduction-band values.

[f] Smith's data have been corrected for strain.

anisotropy, indicating that other mechanisms such as compositional inhomogeneities and distributions of hyperfine couplings owing to local defects in the alloys must be considered. No further study of these issues was carried out.

B. Hyperfine Constants

In the fitting procedure discussed in Sec. V A 3, the hyperfine constants emerge as experimentally determined parameters in the following way: In PbTe, where there is ample data on both n-type and p-type material, the L_6^+ and L_6^- hyperfine constants A_c^{Pb} and A_0^{Pb} are obtained from the slopes of the Knight shift versus $n^{1/3}$ plots in the limit of n approaching zero. In the alloys, the ratio of A_c^{Pb} to A_0^{Pb} was assumed to be the same as the ratio found in PbTe, but both constants were scaled as required to fit the observed data. This assumption of constancy in the ratio is not unreasonable, because this ratio, among other things helps determine the position of the maximum in the Knight shift versus carrier concentration. Experimentally, this maximum does not shift appreciably with composition.

The Sn^{119} hyperfine constants were obtained by using the set of $\vec{k}\cdot\vec{p}$ parameters found from the Pb^{207} data. Since the maximum in the Sn^{119} Knight shift versus carrier concentration occurs at a different carrier concentration than the Pb^{207} maximum it was necessary to increase the ratio of A_c^{Sn} to A_0^{Sn} by a factor of 3.2 over the corresponding ratio for Pb^{207}. Once this was done, the overall values of A_c^{Sn} and A_0^{Sn} at each composition were scaled as needed to yield agreement with the data.

The hyperfine constant obtained in this way can be compared with estimates derived from optical spectra. We will consider first the Pb^{207} hyperfine constant in pure PbTe. The hyperfine constant A_c^{Pb} in PbTe determined from the fit of the experimental data is found to be

$$A_c^{Pb} = \tfrac{8}{3}\pi |\psi(0)|^2_{Pb}\Omega = 1.25\times 10^5 . \tag{13}$$

Using the unit cell volume $\Omega = 6.70\times 10^{-23}$ cm^{-3}, we obtain

$$|\psi(0)|^2_{Pb} = 2.2\times 10^{26}\ \text{cm}^{-3} . \tag{14}$$

For comparison we note that Schawlow *et al.*[56] have deduced from spectroscopic data, the value of the hyperfine coupling constant for a Pb_{6s} state on the Pb^{+3} ion. The wave-function density at the nucleus derived from their Pb^{+3} hyperfine constant is

$$|\psi(0)|^2_{Pb^{+3}} = 6.0\times 10^{26}\ \text{cm}^{-3} . \tag{15}$$

To compare this value with the PbTe experimental value, one must take into account differences in ionicity between Pb in PbTe and Pb^{+3}. Bailey[57] has made two different estimates of ionicity, and has then invoked the Goudsmit–Fermi–Segre formula to calculate a correction factor to apply to the Pb^{+3} value of $|\psi(0)|^2$. The first estimate was based on the APW band calculations.[4,5] Bailey integrated the charge density inside the Pb APW sphere to find a net charge of +1.7 inside this sphere (radius $3.1a_B$). Using +1.7 as the ionicity, Bailey found that the $Pb^{+1.7}$ wave-function density should be smaller than the Pb^{+3} wave-function density by a factor of 2.2. Applying this factor to Eq. (15) yields 2.7×10^{26} cm^{-3} for $|\psi(0)|^2$ to be compared with the experimental PbTe value of 2.2×10^{26} cm^{-3}. It has been pointed out, however, that the Herman–Skillman free atom has +1.3 units of charge inside the volume of the Pb APW sphere.[58,59] and that Bailey's method would therefore attribute an ionicity of +1.3 to the free Pb atom.

Bailey made another estimate of ionicity from the static and optical dielectric constant using the Szigeti relation. The resulting value was +1.4. The Goudsmit–Fermi–Segre formula yields in this case a correction factor of 2.8 from Pb^{+3} to $Pb^{+1.4}$. Applying this factor to Eq. (15) yields

$$|\psi(0)|^2 = 2.1\times 10^{26}\ \text{cm}^{-3} , \tag{16}$$

in very close agreement with the experimental PbTe value. Thus the magnitude of the contact interaction hyperfine constant for PbTe is consistent with estimates based on atomic data.

In the alloys we find a dramatic reduction (nearly a factor of 2) in the Pb contact interaction between pure PbTe and alloys with as little as 17% SnTe. A value of the hyperfine constant ($A_0^{Pb} = 0.72\times 10^4$) typical of the alloy samples corresponds to a wave-function density of 1.3×10^{26} cm^{-3}. This reduction of the wave-function density at the Pb nucleus in the alloys is not yet understood.

We have found a surprisingly large value for the orbital hyperfine constant A_0^{Pb}. For a free atom Kopfermann[60] has estimated that the strength of the hyperfine interaction for a p state ranges from $\frac{1}{5}$ to $\frac{1}{12}$ of the contact interaction of the s state from the same shell. In PbTe we have found an experimental value for the orbital hyperfine constant:

$$A_0^{Pb} = 5.0\times 10^4 . \tag{17}$$

This value is only a factor of 2.5 smaller than the contact term. For the sake of comparison to atomic calculations, we use Eq. (11) to derive a value of $\langle 1/r^3\rangle$ from our experimental value of A_0^{Pb}:

$$\langle X^+|1/r^3|X^+\rangle = 1.5\times 10^{27}\ \text{cm}^{-3} . \tag{18}$$

We have computed $\langle 1/r^3\rangle$ using the Herman–Skillman $6p$ state in atomic lead. The result was $\langle 1/r^3\rangle = 10^{26}$ cm^{-3}, which is an order of magnitude smaller than our experimental value. In these estimates we have not attempted to account for

ionicity or to use relativistic wave functions. Both of these considerations would increase the atomic estimate of $\langle 1/r^3 \rangle$ toward better agreement with the experimental value.

We turn now to Sn. The experimental resolution does not permit any judgement about the composition dependence of the Sn hyperfine constants. Using a typical experimental value for the contact interaction ($A_c^{Sn} = 0.72 \times 10^5$) we obtain an estimate for the Sn 5s wave-function density at the nucleus in the alloys:

$$|\psi(0)|^2_{Sn\,5s} = 1.3 \times 10^{26}\ \text{cm}^{-3}. \quad (19)$$

This value happens to equal to the Pb 6s wave-function density in the alloys. We have no other experimental value on Sn for comparison. However, Knight[61] estimated that the wave-function densities for triply ionized Pb and Sn should be approximately equal. Whether this equality should be expected to hold for Pb and Sn in $Pb_{1-x}Sn_xTe$ is a matter of speculation.

The Sn orbital hyperfine constant needed to fit the Sn NMR data were scaled down by a factor of 3 relative to the corresponding Pb orbital hyperfine constants. This reduction is entirely consistent with the notion that the orbital hyperfine constant arises from spin-orbit unquenching of an L_6^- level, since the local spin-orbit effects should be smaller for Sn than for Pb. Any relativistic enhancement of the expectation value of $\langle 1/r^3 \rangle$ can also be expected to be smaller locally for Sn than for Pb. This difference between the behavior of the Pb and Sn hyperfine constants for the band corresponding to the PbTe conduction band strongly supports the identification of this band as L_6^-.

C. Temperature Dependence in PbTe

An attempt was made to account for the temperature dependence of the Knight shift in PbTe by extending the low-temperature $\vec{k} \cdot \vec{p}$ band model to higher temperatures. The principal effect of an increase in temperature is the shift from degenerate to nondegenerate carrier statistics, i.e., the Fermi level moves out of the band. Explicit calculations of the effect of Fermi level motion were reported earlier,[15] using an algorithm for calculating the Knight shift similar to the approach usually taken in metals. Landau quantization is ignored, and the spin polarization of the carriers in a magnetic field is accounted for with an effective g factor. This approach is very successful as long as the temperature is not so low that de Haas–van Alphen-type Knight shift oscillations occur, and as long as the principal gap is much greater than the Fermi energy, allowing the admixture of conduction-band wave function into the valence band to be accounted for in an approximate way. A calculation similar to that reported previously[15] was made for the data in the present paper. The results are summarized below.

If the $\vec{k} \cdot \vec{p}$ parameters and band-edge hyperfine constants of Table II are used along with the temperature dependence of the principal gap given in Sec. V A 1, and if an effective g factor is used to account in an approximate way for the spin polarization, the predicted temperature dependence of the Knight shift in p-type PbTe between 0 and 300 K is shown in Fig. 7. Note that the effect of the motion of the Fermi level, is as expected, a general decrease in the magnitude of the Knight shift as a function of temperature. The calculated curves agree quite well with experiment for temperatures below about 100 K. Above that temperature there is a systematic failure of the theory in overestimating the Knight shift. A similar error occurs in attempting an extrapolation on the low-temperature theory for n-type PbTe to temperatures above about 100 K.

A secondary valence-band maximum[53,62] has often been invoked in the literature to account for otherwise unexplained features of transport data in PbTe. We investigated whether Allgaier's postulate of such a second valence band could indeed account for the observed variation to no avail. Using Allgaier's[20,53] estimate of an effective mass of $1.2m_0$, and a temperature-dependent energy separation between the principal valence band and the L_6^+ band of $0.14-2.2kT$ eV, and ascribing zero Knight shift to carriers in the second band (see below), new curves for the temperature dependence of the Knight shift were calculated. These calculated curves failed to agree with experiment in a different way: At low carrier concentrations the second band had no effect, leaving the error of Fig. 7 unchanged, while at high carrier concentrations, the second band brought the calculated curves well below the experiment. Thus, a second band cannot be used to account for the varia-

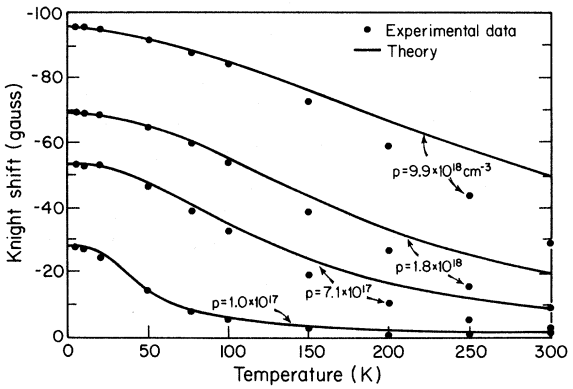

FIG. 7. Temperature dependence of the Knight shift for selected carrier concentrations in p-type PbTe. The solid curves are calculated using the method of Ref. 15.

tion of the Knight shift with carrier concentration at the higher temperatures. We also note that the second valence band calculations have no effect in resolving the similar discrepancy between theory and experiment in n-type PbTe.

The justification for ascribing zero Knight shift to carriers in the second band was as follows: The s character of any state in the zone is likely to be much less than the 96% s character of the states at the L_6^+ band edge. In addition, the effective g factor in a heavy-mass band is likely to be considerably less than the value of 24 for the L_6^+ band edge. Therefore, if there is a Knight shift from such carriers, it must be substantially smaller per carrier than the Knight shift from the extremum around L_6^+. As a first approximation, we assumed zero Knight shift per carrier. Refinements of this estimate are not justified by the failure of this approach at low carrier concentrations. Thus, on the basis of our data, we cannot support the existence of a secondary valence band maximum; nor can we find cause to deny its existence.

Recognizing that other features in the band structure besides the principal gap might be changing with temperature, we investigated whether moderate changes in the principal momentum matrix elements with temperature might improve the agreement between theory and experiment. While the physical interpretation of such *ad hoc* adjustments of parameters is risky at best, it is useful to know whether the results at 300 K can be better described using a band model with different masses and g factors. Surprisingly enough, by reducing $|v_t|^2$ and $|v_1|^2$ by as little as 25%, calculated curves of the Knight shift versus carrier concentration fit the 300 K data fairly well, certainly better than the curves calculated using a second valence band. Nevertheless, in the absence of clear experimental reasons for adjusting these particular quantities (and not others), caution must be exercised in viewing this result. One note of caution has already appeared in the literature. Alexander *et al.*[63] have reported measurements of the Pb^{207} spin-lattice relaxation time in PbTe. They find that the temperature dependence of the relaxation time, when coupled with the temperature dependence of the Knight shift in a Korringa relation, is not consistent with changing the principal matrix elements in the fashion indicated above. This result suggests that the widespread practice of lumping the temperature dependence of transport data into a temperature-dependent effective masses and energy gaps should likewise be treated with caution.

D. Temperature Dependence in the Band Inversion Region

The anomalous structure in the temperature dependence of the Knight shifts in $Pb_{1-x}Sn_xTe$ appear on a background of a general decrease with increasing temperature similar to that observed in PbTe. Two separate attempts were made to account for the anomalous structure. First, it was noted that the width of the anomalous region was roughly proportional to the temperature at which the band inversion occurs. Indeed, assuming a temperature dependence of 4.8 meV/K for the principal gap, the width of the anomalous region corresponds roughly to energy gaps within kT_c of zero, where T_c is the inversion temperature for the particular composition of interest. This fact suggested that the tail of the Fermi distribution might, for very small gap and small carrier concentrations, produce a non-negligible pocket of electrons in the conduction band. Explicit calculations for a sample with 4.5×10^{18} carriers cm^{-3}, however, showed that the Fermi level remains sufficiently far from the band edge to make this effect totally negligible.

The second attempt involved relating the structure to anomalies in the density of states caused by Landau levels moving through the Fermi surface. Explicit calculations showed that even though the Landau level splitting near the band edge gets large when the gap goes to zero, the Fermi level moves away from the band edge. Thus, the Landau levels near the Fermi level move slowly relative to the Fermi level as the gap goes through zero. When the width of the Fermi population factor is included, no structure is observed in calculations of Knight shift versus energy gap, even for carrier concentrations as low as 4×10^{18} cm^{-3}.

At this point, we do not know the source of these anomalies. Experiments specifically devoted to clarifying this issue are currently in progress.

VI. DISCUSSION AND SUMMARY

The experiments reported here, and the extensive successful use of $\vec{k}\cdot\vec{p}$ theory for their interpretation have led us in a number of different directions. First, a detailed $\vec{k}\cdot\vec{p}$ band model was successfully employed to relate the results of Knight shift measurements to other published data on the PbTe and $Pb_{1-x}Sn_xTe$ band structures. Indeed, given the diversity of the sources of experimental data, and considering the complexity of the theory for the magnetic energy levels, it would not have been a surprise to find that no single set of $\vec{k}\cdot\vec{p}$ parameters would suffice to represent all the available data. That such a set could be found for PbTe attests both to the soundness of the model and to the quality of the experiments on which it is based. Furthermore, the quantitative picture that emerges from our analysis is that aside from a variations in far-band couplings of a size entirely consistent with expected variations in far-band energy gaps, the $Pb_{1-x}Sn_xTe$ alloys at least up to $x=0.6$, form a single family of closely related

materials. Indeed, given that the electronegativities of Pb and Sn are identical, one would expect contributions to electron energies based on bonding overlap to be very similar in all the alloys. The variation in principal energy gap can be understood in terms of Dimmock, Melngailis, and Strauss's original proposal,[9] that the energy of the L_6^+ level is most strongly dependent on relativistic contributions (including spin-orbit energy), and as Sn replaces Pb, the effective relativistic energy decreases, raising the energy of the L_6^+ level above that of the L_6^- level.

Several unanswered questions remain. First, the magnitudes of the orbital hyperfine constants are substantially larger than values estimated from atomic data. Furthermore, because the Knight shift in this semiconductor system can be measured directly without having to estimate a reference field, and because the theory involves a small, well characterized region of k space, the interpretation of the experimental values for the hyperfine constants obtained here can be more critical than in the corresponding case of Knight shifts in metals. Thus our inability to account quantitatively for the size of the orbital hyperfine constants with simple atomic estimates underscores the need for more detailed studies of the hyperfine couplings themselves. The observation in the alloys that the hyperfine constants are composition dependent further underscores this need.

In the area of temperature dependence, the low-temperature band model cannot be satisfactorily extrapolated to higher temperatures unless one is willing to ascribe an explicit temperature dependence to the $\vec{k}\cdot\vec{p}$ couplings, a fitting procedure with an unclear physical interpretation. More interesting perhaps is the observation of unexplained anomalies in the Knight shift near the proposed alloy band inversions. Even our rather elaborate $\vec{k}\cdot\vec{p}$ band model fails to account for this behavior. There is clearly a need for more experimental and theoretical studies of the behavior of these and related materials in the band inversion region.

ACKNOWLEDGMENTS

The authors wish to thank Professor Arthur C. Smith for his persistent counsel throughout this work, and Professors Mildred Dresselhaus, George Pratt, and Peter Wolff for valuable suggestions. The assistance of Dr. Alan Strauss, Dr. T. C. Harman, and Dr. James Walpole of the MIT Lincoln Laboratory, and of Dr. Joseph Wrobel of Texas Instruments, and helpful correspondence and discussions with Dr. Bernard Sapoval are gratefully acknowledged.

---

*Work supported by Office of Naval Research and Advanced Research Projects Agency.

†This paper is based in part on the Ph.D. theses of C. R. Hewes (MIT, 1970) and M. S. Adler (MIT, 1971).

‡Present address: General Electric Company, Schenectady, N. Y.

[1]C. R. Hewes, Ph.D. thesis (MIT, 1970) (unpublished).

[2]M. S. Adler, Ph.D. thesis (MIT, 1971) (unpublished).

[3]M. S. Adler, C. R. Hewes, and S. D. Senturia, preceding paper, Phys. Rev. B 7, 5186 (1973).

[4]J. B. Conklin, Jr., L. E. Johnson, and G. W. Pratt, Jr., Phys. Rev. **137**, A1282 (1965).

[5]S. Rabii, Phys. Rev. **167**, 801 (1968).

[6]P. J. Lin and L. Kleinman, Phys. Rev. **142**, 478 (1966).

[7]R. L. Bernick and L. Kleinman, Solid State Commun. **8**, 569 (1970).

[8]Y. W. Tung and M. L. Cohen, Phys. Rev. **180**, 823 (1969).

[9]J. O. Dimmock, I. Melngailis, and A. J. Strauss, Phys. Rev. Lett. **16**, 1193 (1966).

[10]I. Weinberg, J. Chem. Phys. **36**, 1112 (1962).

[11]I. Weinberg, J. Chem. Phys. **39**, 492 (1963).

[12]I. Weinberg and J. Callaway, Nuovo Cimento **24**, 190 (1962).

[13]B. Sapoval, Phys. Rev. Lett. **17**, 241 (1966).

[14]B. Sapoval, thesis (Ecole Polytechnique, 1967) (unpublished); J. Phys. (Paris) Suppl. **29**, C4-133 (1968).

[15]S. D. Senturia, A. C. Smith, C. R. Hewes, J. A. Hofmann, and P. L. Sagalyn, Phys. Rev. B **1**, 4045 (1970).

[16]S. D. Senturia, A. C. Smith, C. R. Hewes, M. S. Adler, J. A. Hofmann, and P. L. Sagalyn, J. Phys. Chem. Solids Suppl. **32**, 333 (1971).

[17]K. Lee, J. Liesegang, and P. B. P. Phipps, Phys. Rev. **161**, 322 (1967).

[18]B. Sapoval (private communication).

[19]C. R. Hewes, M. S. Adler, and S. D. Senturia, J. Appl. Phys. **44**, 1327 (1973).

[20]R. S. Allgaier, J. Appl. Phys. **32**, 2185 (1961).

[21]M. S. Adler, S. D. Senturia, and C. R. Hewes, Rev. Sci. Instrum. **42**, 704 (1971).

[22]M. S. Adler, U.S. Patent No. 3 548 298.

[23]D. B. Utton, Metrologia **3**, 98 (1967).

[24]H. M. Gibbs and C. M. Whitt, Phys. Rev. **188**, 180 (1969).

[25]H. M. Gibbs, B. Chang, and R. C. Greenhaw, Phys. Rev. **188**, 172 (1969).

[26]L. Pauling, *The Nature of the Chemical Bond* (Cornell U. P., Itahca, N. Y., 1960).

[27]Y. Yafet, J. Phys. Chem. Solids Suppl. **21**, 99 (1961).

[28]D. L. Mitchell and R. F. Wallis, Phys. Rev. **151**, 581 (1966).

[29]W. M. Shyu, T. P. Das, and G. D. Gaspari, Phys. Rev. **141**, 603 (1966).

[30]P. Jena and T. P. Das, Phys. Rev. B **1**, 432 (1970).

[31]G. D. Gaspari, W. M. Shyu, and T. P. Das, Phys. Rev. **134**, A852 (1964).

[32]D. L. Mitchell, E. D. Palik, and J. N. Zemel, in *Proceedings of the International Conference on the Physics of Semiconductors* (Dunod Cie, Paris, 1964), p. 325.

[33]J. F. Butler and A. R. Calawa, *Physics of Quantum Electronics*, edited by P. L. Kelley, B. Lax, and P. E. Tannenwald (McGraw-Hill, New York, 1966), p. 458.

[34]K. U. H. Smith, Ph.D. thesis (MIT, 1971) (unpublished).

[35]J. F. Butler and T. C. Harman, Appl. Phys. Lett. **12**, 347 (1968).

[36]J. F. Butler, A. R. Calawa, and T. C. Harman, Appl. Phys. Lett. **12**, 427 (1966)

[37]J. F. Butler, Solid State Commun. **7**, 909 (1967).

[38]J. R. Dixon and R. F. Bis, Phys. Rev. **176**, 942 (1968).

[39]L. Esaki and P. J. Stiles, Phys. Rev. Lett. **16,** 1108 (1966).
[40]J. R. Burke, Jr. and H. R. Riedl, Phys. Rev. **184,** 830 (1969).
[41]R. N. Tauber, A. A. Machonis, and I. B. Cadoff, J. Appl. Phys. **37,** 4855 (1966).
[42]E. R. Washwell and K. F. Cuff, in *International Conference on the Physics of Semiconductors* (Academic, New York, 1964).
[43]A. F. Gibson, Proc. Phys. Soc. Lond. B **65,** 378 (1952).
[44]T. C. Harman, A. R. Calawa, I. Melngailis, and J. O. Dimmock, Appl. Phys. Lett. **11,** 333 (1969).
[45]K. F. Cuff, M. R. Ellett, C. D. Kuglin, and L. R. Williams, in Ref. 32, p. 677.
[46]J. R. Burke, J. Phys. Chem. Solids Suppl. **32,** 393 (1971).
[47]C. K. N. Patel and R. E. Slusher, Phys. Rev. **177,** 1200 (1969).
[48]R. Nii, J. Phys. Soc. Jap. **19,** 58 (1964).
[49]J. N. Walpole and A. L. McWhorter, Phys. Rev. **158,** 708 (1967).
[50]J. Melngailis, T. C. Harman, J. G. Mavroides, and J. O. Dimmock, Phys. Rev. B **3,** 370 (1971).
[51]B. Ellis and T. S. Moss, Phys. Status Solidi **4,** 531 (1970).
[52]J. Melngailis, T. C. Harman, J. G. Mavroides, and J. O. Dimmock, Bull. Am. Phys. Soc. **14,** 330 (1969).
[53]R. S. Allgaier and B. B. Houston, Jr., J. Appl. Phys. **37,** 302 (1966).
[54]B. B. Houston, Jr., R. S. Allgaier, J. Babiskin, and P. G. Siebenmann, Bull. Am. Phys. Soc. **9,** 60 (1964).
[55]R. F. Brebrick and A. J. Strauss, J. Chem. Phys. **41,** 197 (1964).
[56]A. L. Schawlow, J. N. P. Hume, and M. F. Crawford, Phys. Rev. **76,** 1876 (1949).
[57]P. T. Bailey, Phys. Rev. **170,** 723 (1968); and P. T. Bailey, Ph.D thesis (MIT, 1966) (unpublished).
[58]The value of 1.3 is in agreement with results obtained by D. Choo and E. K. Li (private communication).
[59]F. Herman and S. Skillman, *Atomic Structure Calculations* (Prentice-Hall, Englewood Cliffs, N. J., 1963).
[60]H. Kopfermann, *Nuclear Moments* (Academic, New York, 1958).
[61]W. D. Knight, in *Solid State Physics*, edited by F. Seitz and D. Turnbull (Academic, New York, 1956), Vol. II, p. 119.
[62]A. A. Andreev and V. N. Radionov, Fiz. Tekh. Poluprovodn. **1,** 183 (1966) [Sov. Phys.-Semicond. **1,** 145 (1967)].
[63]N. M. Alexander, P. L. Sagalyn, S. D. Senturia and C. R. Hewes, J. Nonmetals (to be published).

PHYSICAL REVIEW B VOLUME 7, NUMBER 12 15 JUNE 1973

Mean-Value Point in the Brillouin Zone

A. Baldereschi
Bell Laboratories, Murray Hill, New Jersey 07974
(Received 6 November 1972)

A new special point in the Brillouin zone is introduced. It is defined as the point such that the value which any given periodic function of wave vector assumes at this point is an excellent approximation to the average value of the same function throughout the Brillouin zone. This special point is termed the "mean-value point," and is dictated by the crystal symmetry. The coordinates of the mean-value point for cubic lattices are explicitly given.

Different kinds of special points in the Brillouin zone have been introduced since the existence of these zones was noticed in 1928.[1] After the work by Bouckaert *et al.*[2] on the symmetry properties of wave functions in crystals, the concept of high-symmetry points in the zone gained large popularity and is still one of the basic concepts in solid-state physics. Later, when deep interest arose in the thermodynamical and optical properties of solids, the concept of phonon (or electron) density of states became relevant and critical points were introduced by Van Hove[3] and studied in more detail by Phillips.[4]

Often, one is not interested in studying the properties of a single quasiparticle which belongs to a particular point of the Brillouin zone, but rather in studying the properties of all the quasiparticles of a certain kind which are present in the crystal in order to obtain crystal properties. In these studies one is usually faced with the problem of averaging quasiparticle properties (i.e., averaging over the Brillouin zone). It is well known that carrying out such averages is difficult and time consuming. It is useful in this respect to introduce a new special point in the Brillouin zone: the mean-value point.[5] Qualitatively, it is defined as the point such that the value which any given periodic function of wave vector assumes at this point is an excellent approximation to the average value of the same function throughout the Brillouin zone. It will be shown that the symmetry properties of crystals provide a way to uniquely define this point for any given lattice. The coordinates of the mean-value point in cubic lattices will be given together with two examples from semiconductor physics which will show how useful this new point can be.

While studying crystal properties, one often encounters Brillouin-zone integrals such as

$$I=\int_{\mathrm{BZ}} f(\vec{k})\,d^3k=\frac{(2\pi)^3}{\Omega}\,\bar{f}\,, \tag{1}$$

where the integrand $f(\vec{k})$ is a periodic function of wave vector and Ω is the primitive cell volume. As shown in (1), this integral can be expressed as the Brillouin-zone volume times the average value of